Supporting Information

Significantly Enhanced Electrocatalytic N_2 Reduction to NH_3 by the Surface Selenization with Multiple Functions

Wenwen Cai[#,a] Yi Han[#,a] Hongdong Li,[a] Wenjing Qi,[b] Jixiang Xu,[a] Xueke Wu,[a] Huan Zhao,[a] Xinyi Zhang,[a] Jianping Lai*[,a] and Lei Wang*[,a]

[a]Key Laboratory of Eco-chemical Engineering, Ministry of Education, Taishan scholar advantage and characteristic discipline team of Eco-chemical process and technology, Laboratory of Inorganic Synthesis and Applied Chemistry, College of Chemistry and Molecular Engineering, Qingdao University of Science and Technology, Qingdao 266042, P. R. China.
[b]College of Chemistry, Chongqing Normal University, Chongqing 401331, P. R. China.

[#]Equal Contribution

Experimental Section

Materials. $RuCl_3$, Se, Li_2SO_4, NaOH, D_2O (99.9 atom%), DMSO (99.95%) and $NaBH_4$ were supplied by Aladdin (Shanghai, China). HCl was purchased from Far East Fine Chemicals (Yantai, China). NH_4Cl was obtained from Tianjin Bodi Chemical Co., Ltd. China. $^{15}NH_4Cl$ (99 atom%) was supplied by Morai Chemical. All the chemicals were analytical-reagent grade and used without further purification.

Preparation of RuO_2/C. Specifically, a certain amount of Carbon (30 mg) and $RuCl_3$ were added into an agate mortar and grounded together for 30 minutes. Thereafter, 0.016 g of NaOH and 0.0152 g of $NaBH_4$ were added, after the ground for 30 minutes respectively. The resulting powder was centrifuged several times in a centrifuge until the solution pH = 7. The samples were then dried at 60 ℃.

Preparation of RuO_2-Se_x/C. 10 mg of the obtained RuO_2 powder was transferred into a magnetic boat and flattened. Then 100 mg of selenium powder is spread in another magnetic boat. Then magnetic boats were calcined at 250 ℃, 300 ℃ and 350 ℃ for 2 h with a heating rate of 5 ℃/min, respectively. After being cooled to room temperature, the resulting products were collected.

Preparation of $RuSe_2$/C. 10 mg of the obtained RuO_2 powder was transferred into a magnetic boat and flattened. Then 100 mg of selenium powder is spread in another magnetic boat. Then magnetic boats were calcined at 600 ℃ for 2 h with a heating rate of 5 ℃/min, respectively. After being cooled to room temperature, the resulting products were collected.

Preparation of C-Se: 10 mg carbon was transferred into a magnetic boat and flattened. Then 100 mg of selenium powder is spread in another magnetic boat. Then magnetic boats were calcined at 300 ℃ for 2 h with a heating rate of 5 ℃/min. After being cooled to room temperature, the resulting products were collected.

Characterization. X-ray diffraction (XRD) analysis at a scanning rate of 1 °min^{-1} in the 2θ ranges from 1 to 80 °was used to examine the composition of the as-synthesized samples on X'Pert PRO MPD. Scanning electron microscopy (SEM) measurement was collected on Hitachi, S-4800 to investigate the structure and morphology of the samples. Transmission electron microscopy (TEM) and high-resolution TEM (HRTEM) measurements were performed on JEM-2100UHR with operating at 200 kV. The X-ray photoelectron spectrum (XPS) was conducted using a VG ESCALABMK II spectrometer with AlKa (1486.6 eV) photon source. All the electrochemical performances of the as-synthesized samples were carried out on an electrochemical station (CHI 760E). The ^{1}H NMR spectrum was recorded on a Bruker 500 with Probe TXI at temperature of 25 ℃ using a 3 mm tube. The electrolyte after electrolysis was collected, lyophilized and further dissolved in 1M HCl solution (D_2O/H_2O mixed solution). The IC date were collected by an IC (863 Basic IC Plus. Metrohm, Switzerland) equipped with a Metrosep C Supp 4-250/4.0 column.

Electrochemical measurements. All electrochemical measurements were performed by using an electrochemical workstation (Shanghai Chenhua Instrument Corporation, China) and a two-compartment electrochemical cell, which was connected with a salt bridge. The RuO_2-Se_x/C dropped on the carbon paper was used as a working electrode, carbon rod as an auxiliary electrode and the saturated calomel electrode (SCE) with a saturated KCl electrolyte as a reference electrode. All the gas used in this work is with a purity grade of 99.999 % and fully purified by the Cu impurity trap, then plunged into the electrolyte more than 30 min. The following equation was used to convert the potential reported in this work to the RHE scale: E(RHE)=E(SCE)+(0.244+0.059×pH)V. For the NRR test, the chronoamperometry experiments were conducted in N_2-saturated 0.1 M Li_2SO_4 solution (Notably, the Li_2SO_4 used was pretreated at 800 ℃ about 4 h in Ar.) with stirring at 450 rpm. For the preparation of the working electrode,

6 mg catalyst was first dispersed in 1.0 mL of absolute ethanol and 50 μL of Nafion solution (5.0 wt%) under ultrasonication for 5 min to form a homogeneous catalyst ink. After that, the as-prepared catalyst ink was completely loaded onto a commercial carbon paper with an area of 1.0×1.0 cm^2, then dried under ambient conditions for use.

Ammonia quantification. The produced NH_3 was quantitatively determined using the indophenol blue method.[1] Typically, 1 mL of the sample solution was first pipetted from the post-electrolysis electrolyte. Afterward, 1 mL of a 1M NaOH solution containing salicylic acid (5 wt%) and sodium citrate (5 wt%) was added, and 0.5 mL of NaClO solution (0.05 M) and 0.1 mL of sodium nitroferricyanide solution (1 wt%) were added subsequently. After 2 h, the absorption spectra of the resulting solution were acquired with an ultraviolet-visible (UV-vis) spectrophotometer (BioTek Synergy H1 Hybrid Multi-Mode Reader). The formed indophenol blue was measured by absorbance at λ = 654 nm. The concentration (NH_4^+) absorbance curve used for estimation of NH_3 amount was calibrated using standard NH_4Cl solution with NH_4^+ concentrations of 0.0, 0.2, 0.4, 0.6, 0.8, and 1.0 μg mL^{-1} in 0.1 M Li_2SO_4. The fitting curve ($y=0.509x+0.04065$, $R^2=0.999$) showed a good linear relation between the NH_4^+ concentration and absorbance.

$^{15}N_2$ isotope labelling experiments. The produced NH_3 was detected by the ^1H NMR. $^{15}N_2$ (99%, provided by the Shanghai Aladdin Biochemical Technology Co., Ltd) was used to further verify the N -source of NH_3 produced. All the gases were purified by the Cu impurity trap. Before the electrolysis, the Ar was plunged into the electrolyte about 1 h, then $^{15}N_2$ was plunged into the electrolyte to saturation. The electrolyte after electrolysis at -0.1 (V vs. RHE) was collected, lyophilized and further dissolved in the solution of 1 M HCl, D_2O and H_2O. Then the $^{15}NH_3$ produced was detected by the ^1H NMR spectrum (Bruker 500). The procedure that detected $^{14}NH_3$ produced was the same except the $^{14}N_2$ (99.999%) was used. The standard curves was calibrated by using a series of concentrations of NH_4Cl And the fitting curves are $y=0.034x+0.004$, $R^2=0.999$ and $y=0.036x-0.002$, $R^2=0.998$.

Determination of hydrazine. The hydrazine present in the electrolyte was estimated by the method of Watt and Chrisp.[2] A mixture of para-(dimethylamino) benzaldehyde (5.99 g), HCI (concentrated, 30 mL) and ethanol (300 mL) was used as a color reagent. The calibration curve was plotted as follow: First, preparing a series of reference solutions, by pipetting suitable volumes of the hydrazine hydrate-nitrogen 0.1 M HCl solution in colorimetric tubes; Second, making up to 5 mL with 0.1 M HCl solution; Third, adding 5 mL above prepared color reagent and stirring 10 min at room temperature; Fourth, the absorbance

of the resulting solution was measured at 455 nm, and the obtained calibration curve (y=1.184x+0.02371, R^2=0.999) was used to calculate the hydrazine concentration.

Calculation of the Faradaic efficiency and the yield rate. The faradaic efficiency for N_2 reduction was defined as the amount of electric charge used for synthesizing NH_3 divided the total charge passed through the electrodes during the electrolysis. The total amount of NH_3 produced was measured using colorimetric methods. Assuming three electrons were needed to produce one NH_3 molecule, the FE could be calculated as follows:

Faradaic efficiency (FE,%)=$(3F \times C_{NH4^+} \times V)/(17Q) \times 100\%$

The NH_3 yield was calculated using the following equation:

NH_3 yield=$(C_{NH4+} \times V)/(t \times A)$

where F is the faraday constant, C_{NH4+} is the measured concentration of NH_4^+, V is the electrolyte volume, Q is the sum of electric charge recorded by electrochemical workstation, 17 is the molarmass of NH_4^+ atom, t is the reaction time, and A is the geometric area of the cathode (1 cm^{-2}).

Calculation Setup. DFT calculations were performed in the Vienna ab initio simulation package (VASP). A spin-polarized GGA PBE functional, all-electron plane-wave basis sets with an energy cutoff of 520 eV, and a projector augmented wave (PAW) method were adopted. RuO_2 and RuO_2-Se_x are simulated using a surface model of p (2 × 2) unit cell periodicity. A (3 × 3 × 1) Monkhorst-Pack mesh was used for the Brillouin-zone integrations to be sampled. The conjugate gradient algorithm was used in the optimization. The convergence threshold was set 1×10^{-4} eV in total energy and 0.05 eV/ Å in force on each atom.

The adsorption energy change (ΔE_{abs}) was determined as follows:

$\Delta E_{abs} = E_{total} - E_{sur} - E_{mol}$

where E_{total} is the total energy for the adsorption state, E_{sur} is the energy of pure surface, E_{mol} is the energy of molecule.

The free energy change (ΔG) for adsorptions were determined as follows:

$\Delta G = E_{total} - E_{sur} + \Delta E_{ZPE} - T\Delta S$

where E_{total} is the total energy for the adsorption state, E_{sur} is the energy of pure surface, ΔE_{ZPE} is the

zero-point energy change and ΔS is the entropy change.

Figures

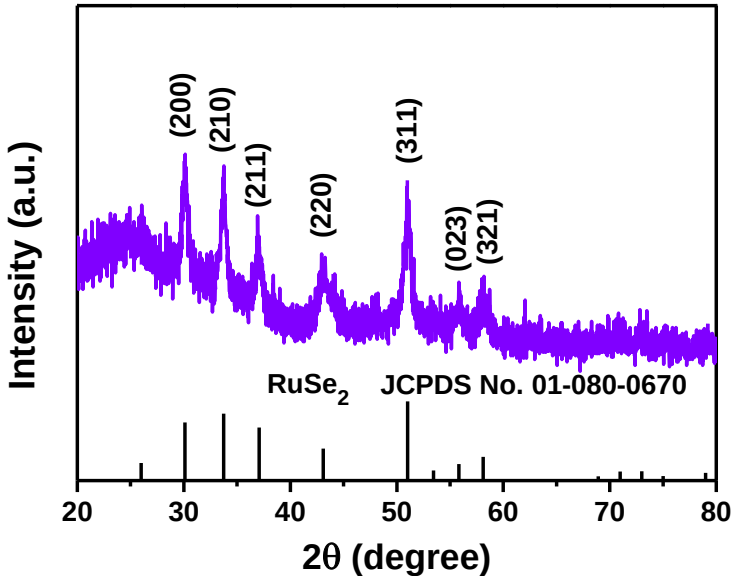

Figure S1. The XRD pattern of $RuSe_2$/C catalyst.

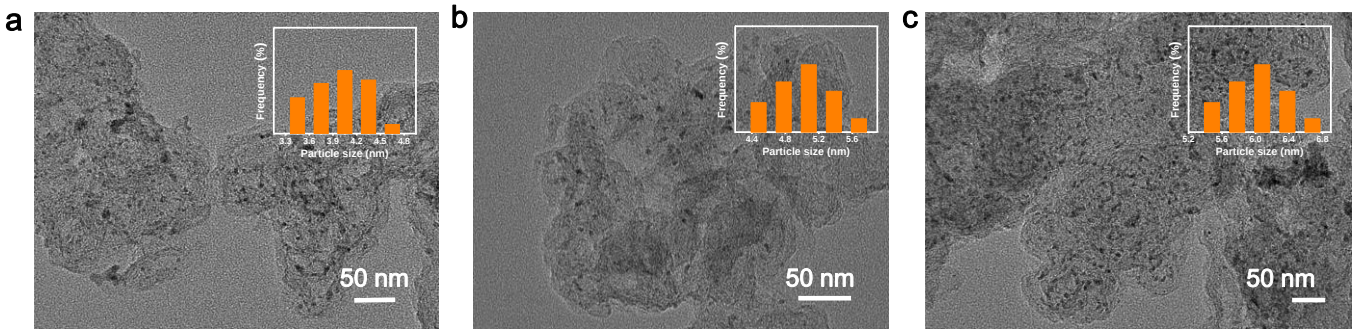

Figure S2. TEM image of (a) precursor RuO_2/C, (b) RuO_2-$Se_{0.06}$/C and (c) RuO_2-$Se_{0.64}$/C.

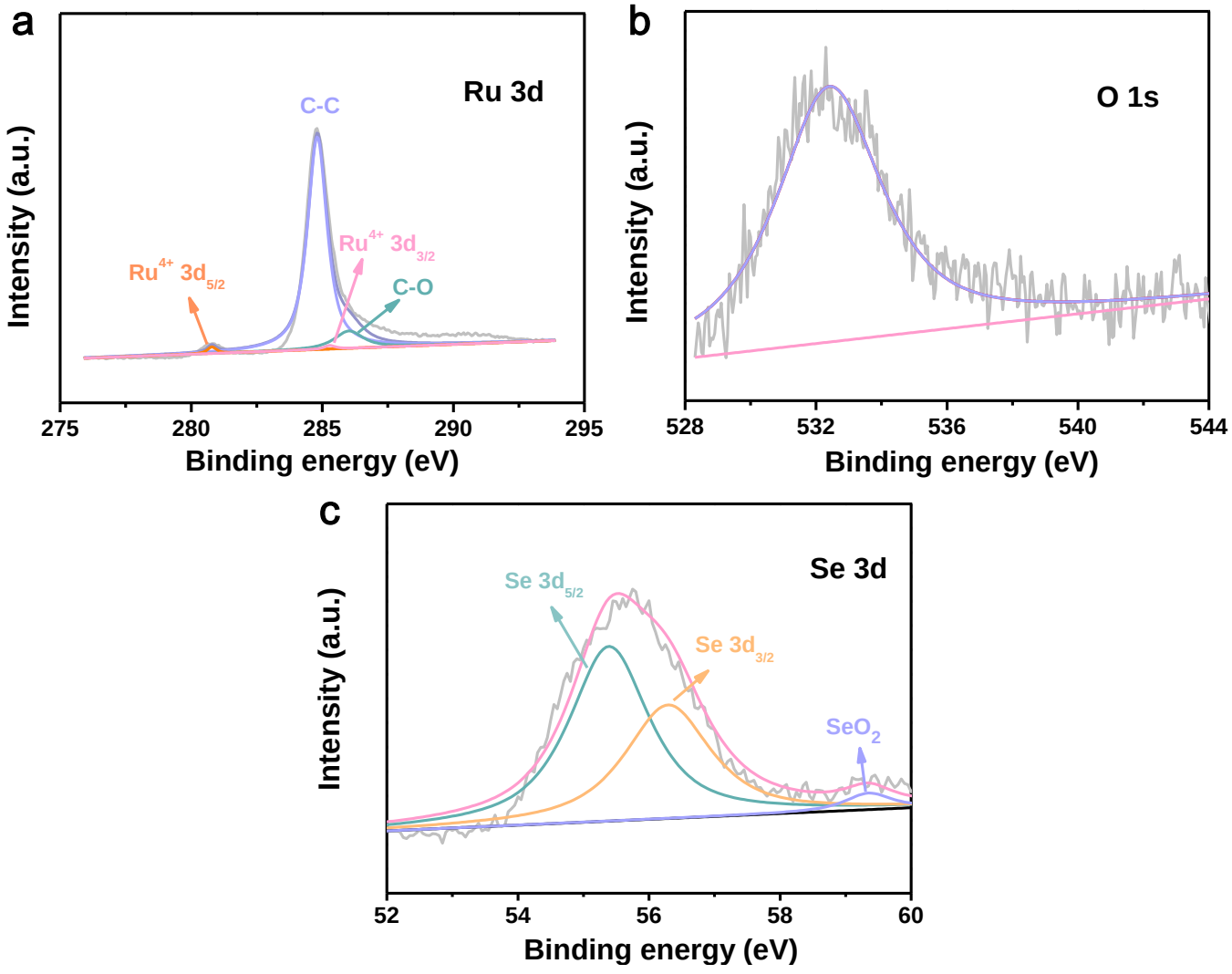

Figure S3. XPS spectra of (a) Ru 3d, (b) O 1s and (c) Se 3d signals in RuO_2-$Se_{0.18}$/C.

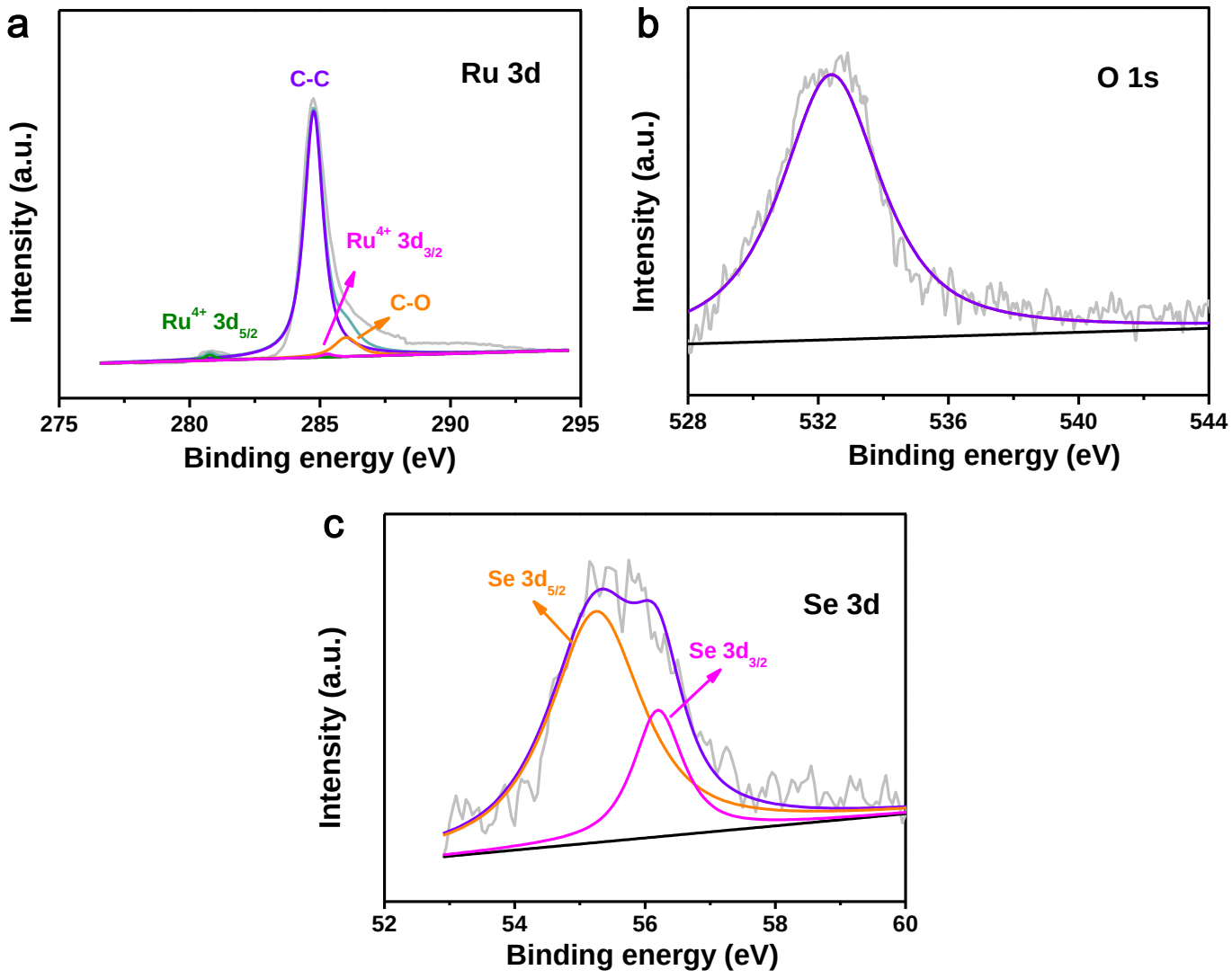

Figure S4. XPS spectra of (a) Ru 3d, (b) O 1s and (c) Se 3d signals in RuO_2-$Se_{0.06}$/C.

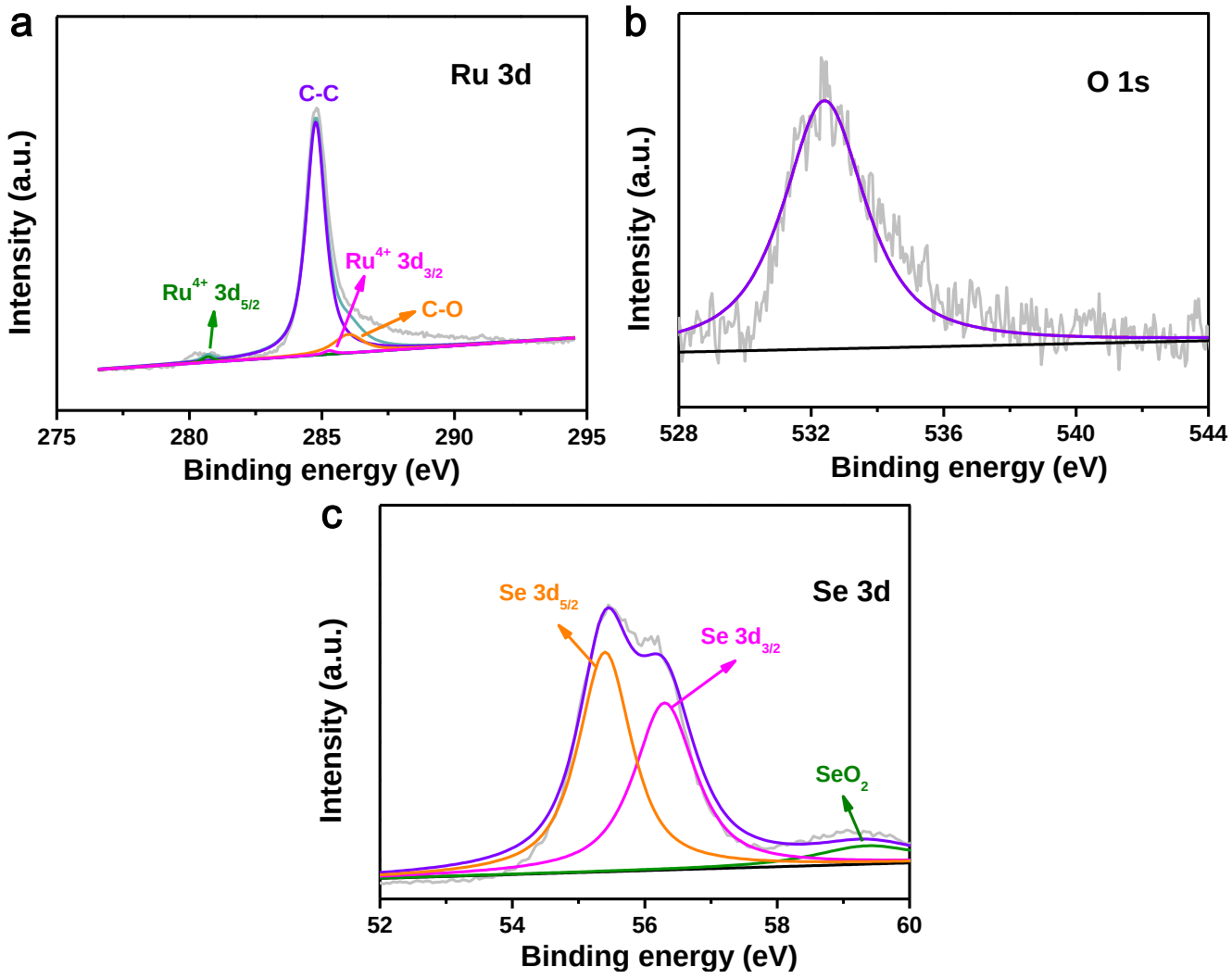

Figure S5. XPS spectra of (a) Ru 3d, (b) O 1s and (c) Se 3d signals in RuO_2-$Se_{0.64}$/C.

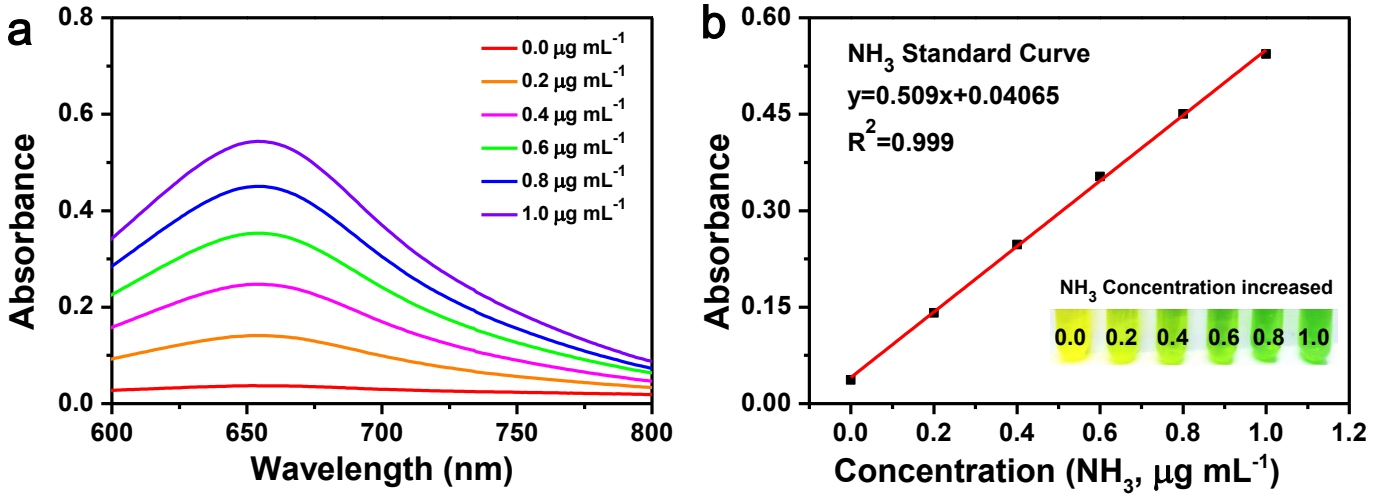

Figure S6. (a) The UV-Vis absorption spectra of indophenol assays with NH_3 after incubated for 2 h at room temperature. (b) Corresponding calibration curves for the colorimetric NH_3 assay in 0.1 M Li_2SO_4.

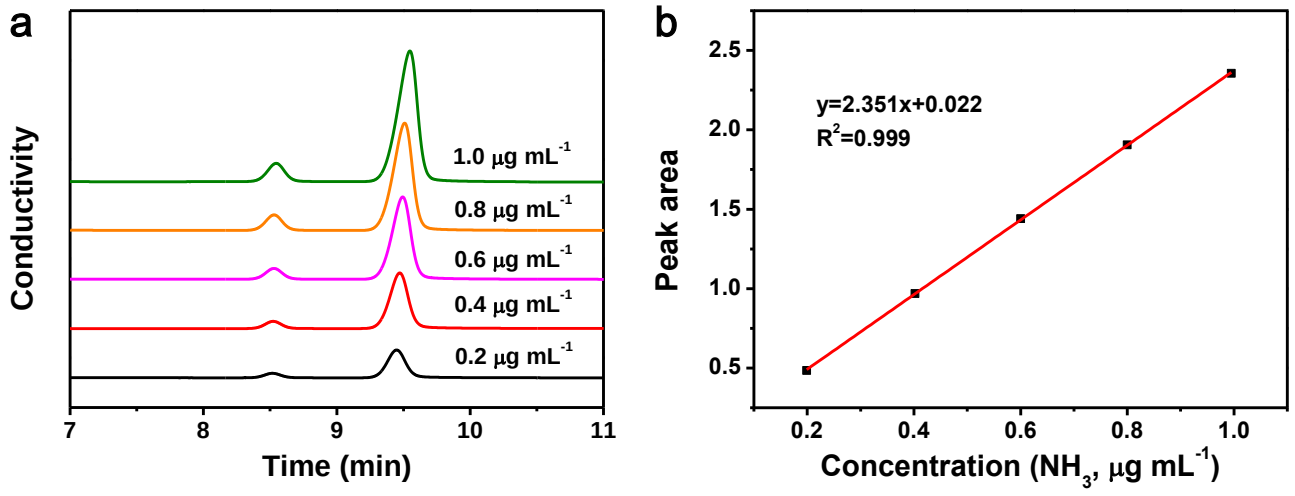

Figure S7. (a) Ion chromatogram analysis for the NH_4^+. (b) Calibration curve used for estimation of NH_4^+.

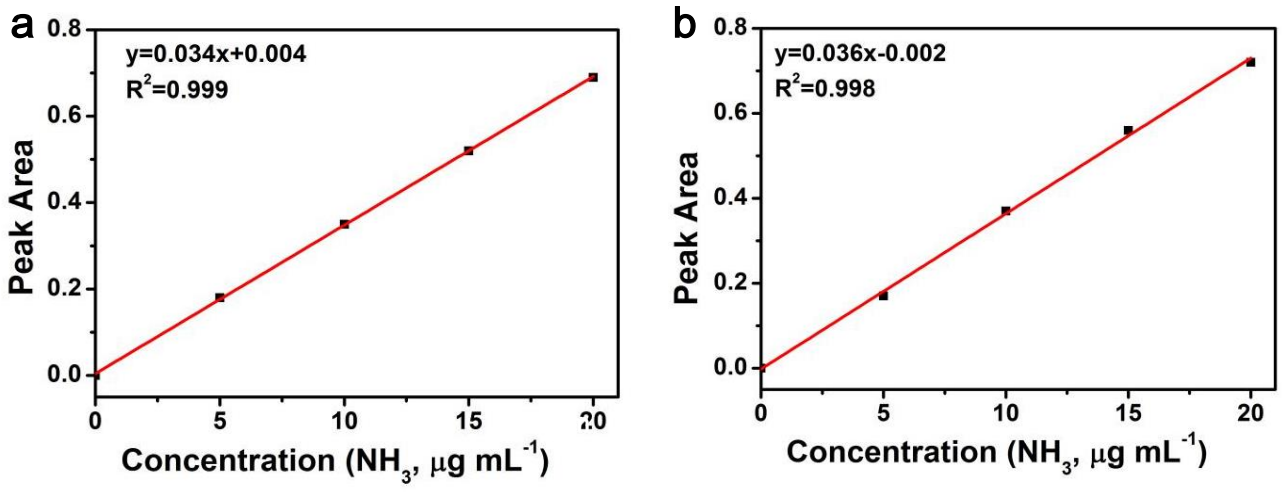

Figure S8. (a) Calibration curves for determination of $^{14}NH_4^+$. (b) Calibration curves for determination of $^{15}NH_4^+$.

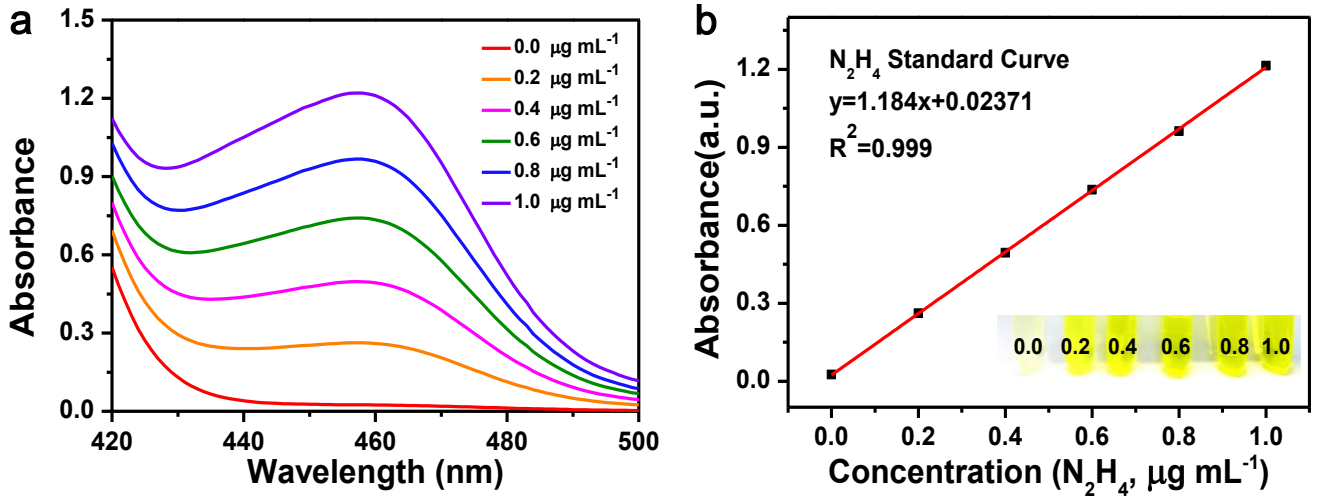

Figure S9. (a) The UV-Vis absorption spectra of indophenol assays with N_2H_4 after incubated for 10 min at room temperature. (b) Corresponding calibration curves for the colorimetric N_2H_4 assay in 0.1 M Li_2SO_4.

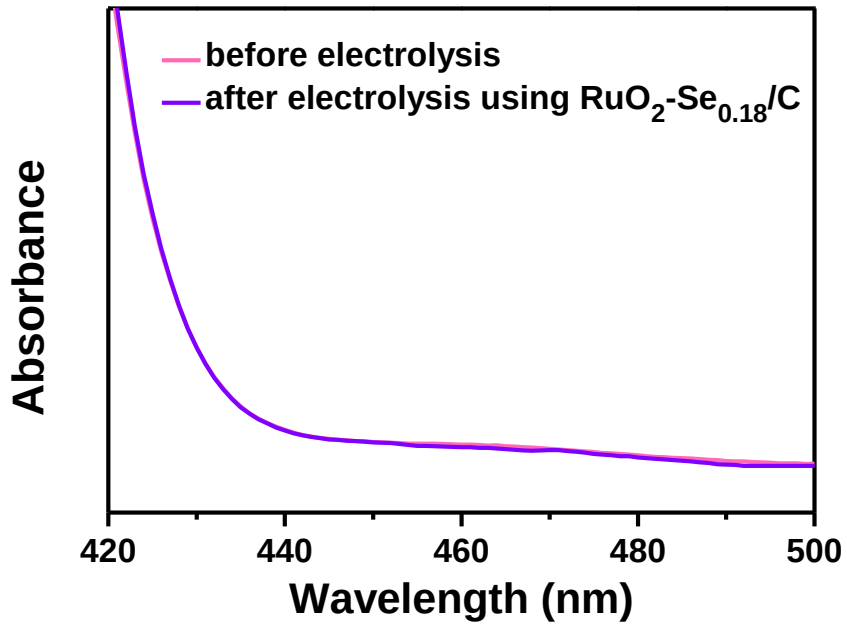

Figure S10. UV-Vis spectra of the electrolyte before and after electrolysis at -0.1 V (vs. RHE).

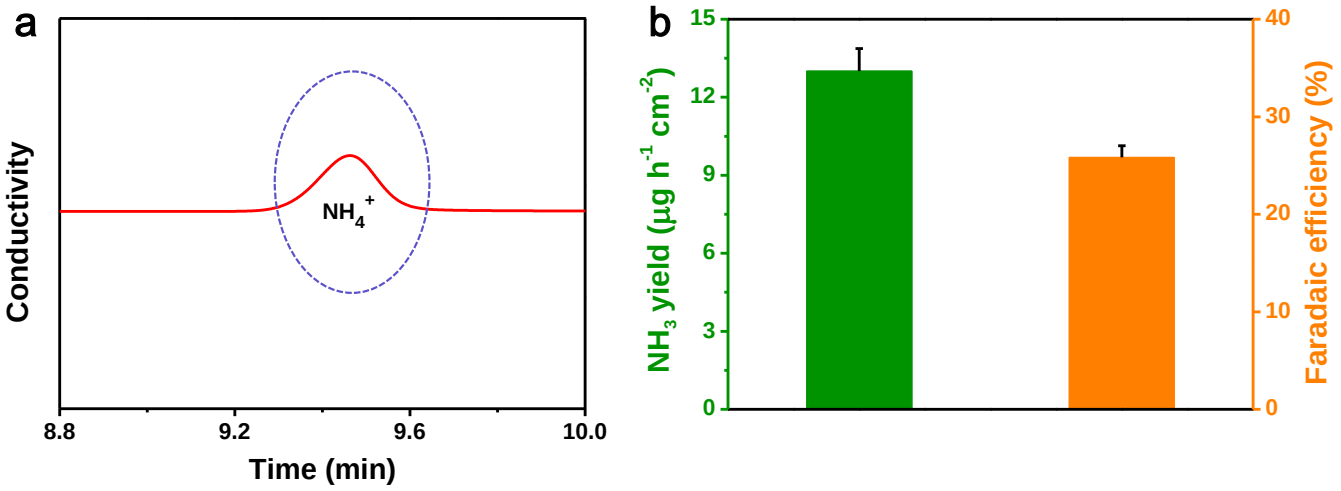

Figure S11. (a) Ion chromatogram analysis for the NH_4^+ of RuO_2-$Se_{0.18}$/C. (b) The NH_4^+ yield and FE detected by ion chromatography.

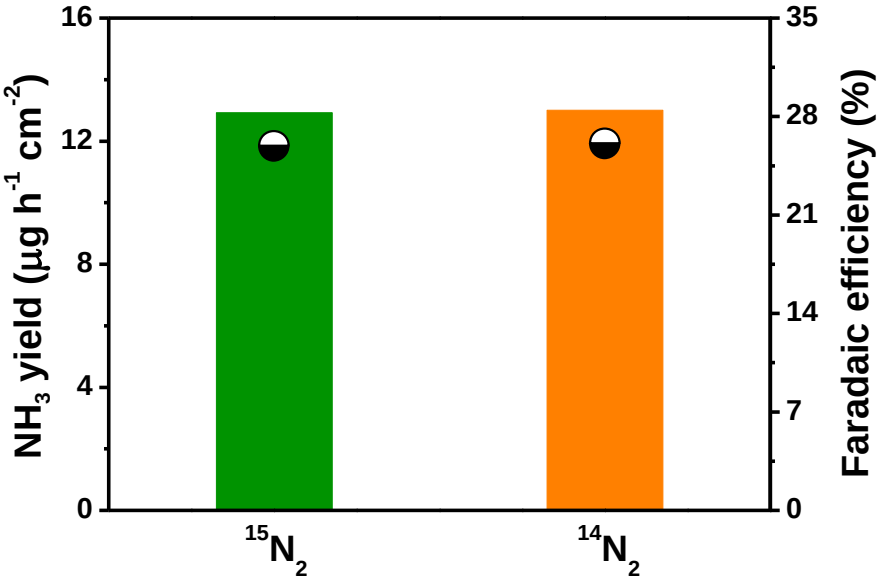

Figure S12. Comparison of the FE and NH_3 yield using different feeding gases for the NRR at -0.1 V (vs. RHE).

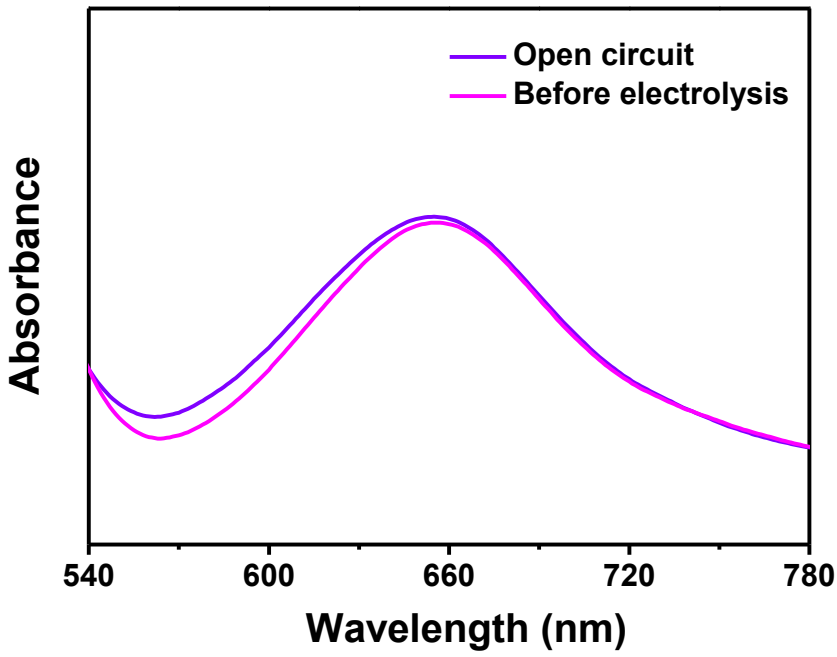

Figure S13. UV-Vis absorption spectra of the electrolyte stained with indophenol indicator before and after electrolysis at -0.1 V (vs. RHE).

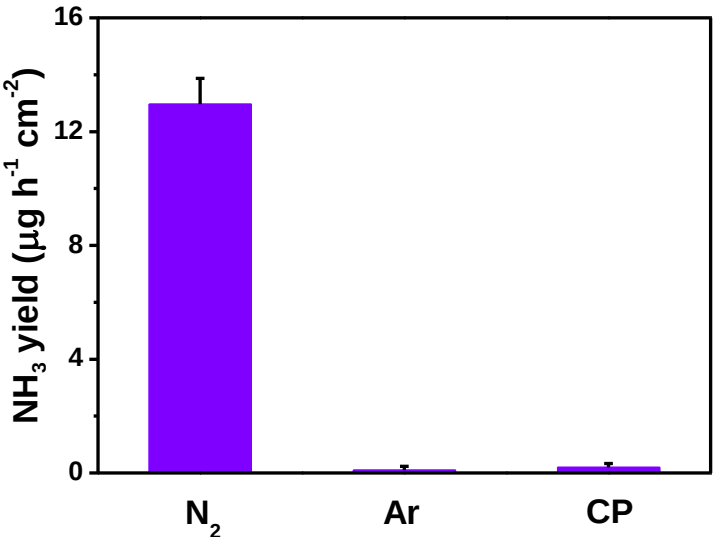

Figure S14. Control tests in 0.1 M Li_2SO_4 solution at -0.1 V (vs. RHE).

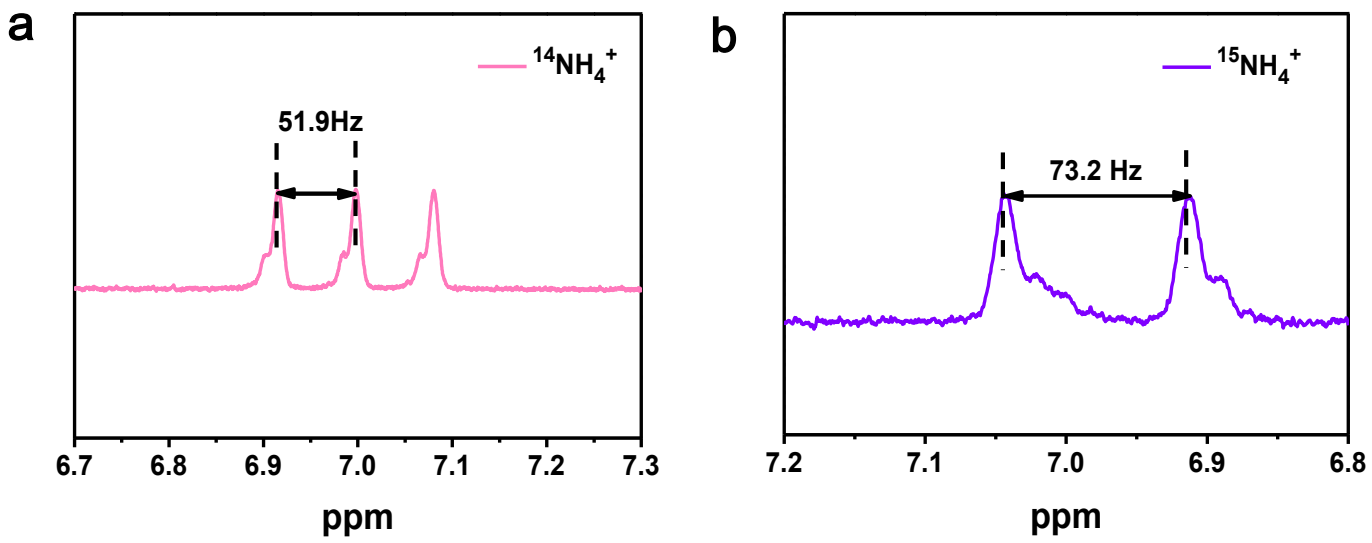

Figure S15. (a) The ^{1}H-NMR spectrum of electrolyte that electrolysis in $^{14}N_2$-saturated condition. (b) The ^{1}H-NMR spectrum of electrolyte that electrolysis $^{15}N_2$-saturated condition.

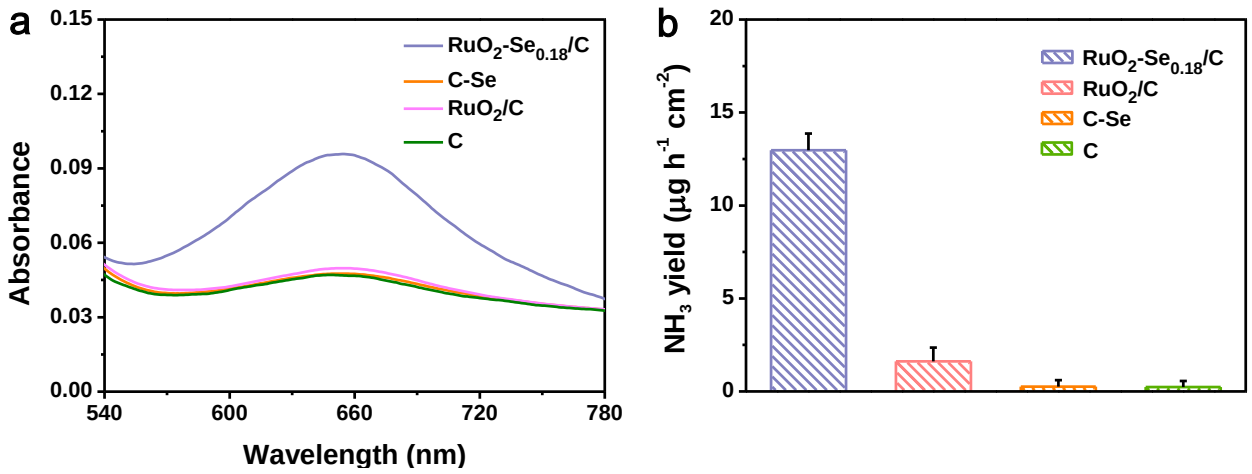

Figure S16. Comparative tests of different catalysts in 0.1 M Li_2SO_4 solution at -0.1 V (vs. RHE).

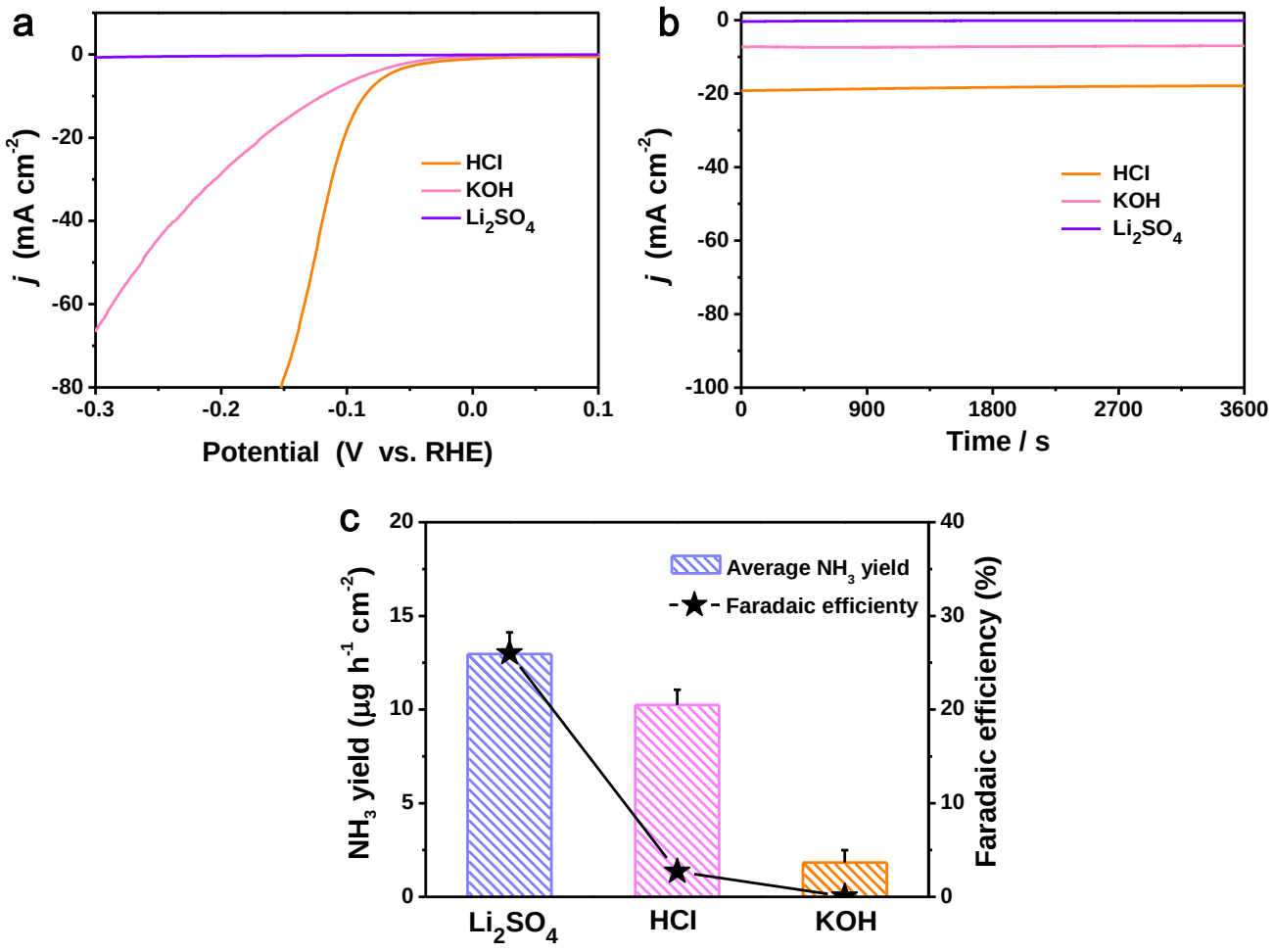

Figure S17. (a) LSV curves of catalysts in three N_2-saturated solutions with a scan rate of 5 mV s^{-1}. (b) Chronoamperometry curves at various potentials in three N_2-saturated solutions. (c) NH_3 yield and FE at -0.1 V (vs. RHE) in three solutions.

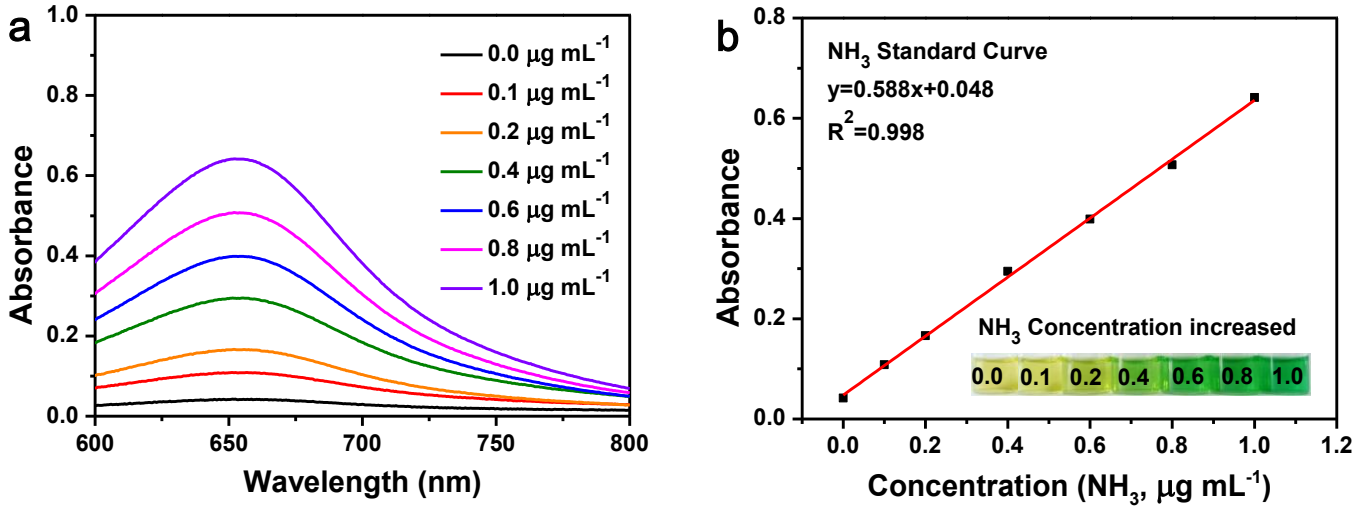

Figure S18. (a) The UV-Vis absorption spectra of indophenol assays with NH_3 in 0.1 M KOH after incubated for 2 h at room temperature. (b) Corresponding calibration curves for the colorimetric NH_3 assay in 0.1 M KOH.

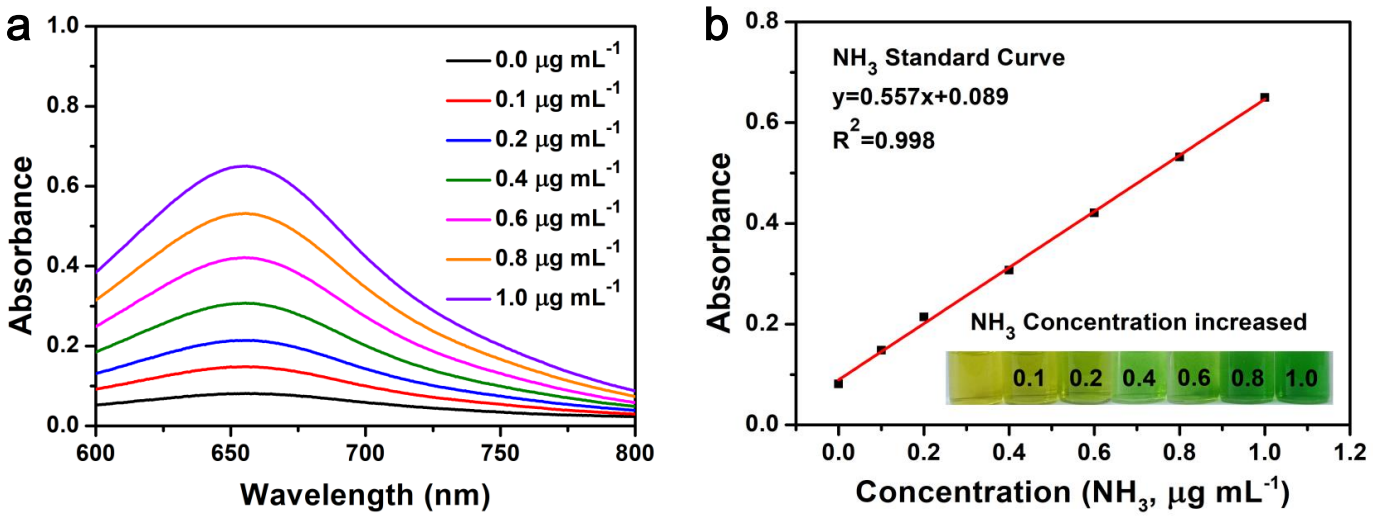

Figure S19. (a) The UV-Vis absorption spectra of indophenol assays with NH_3 in 0.1 M HCl after incubated for 2 h at room temperature. (b) Corresponding calibration curves for the colorimetric NH_3 assay in 0.1 M HCl.

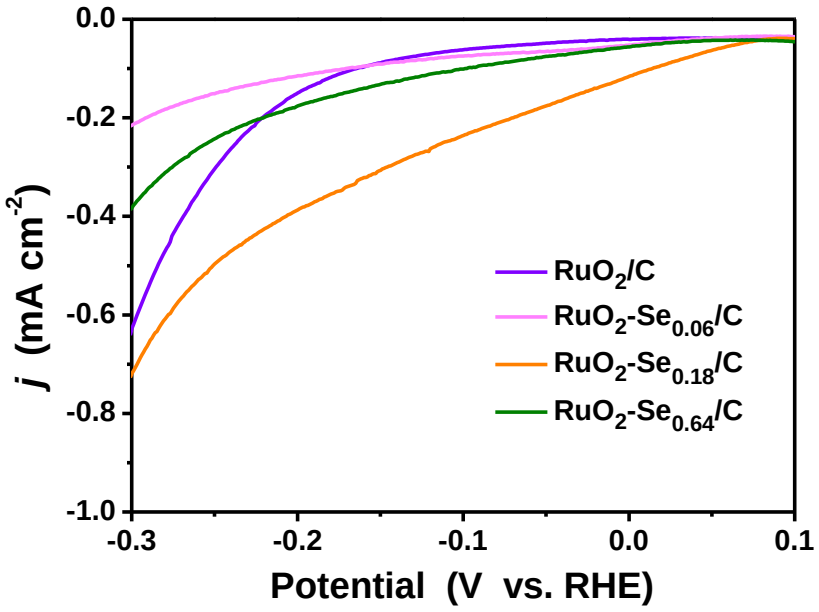

Figure S20. LSV curves of RuO_2/C, RuO_2-$Se_{0.06}$/C, RuO_2-$Se_{0.18}$/C and RuO_2-$Se_{0.64}$/C catalysts in 0.1 M Li_2SO_4 solution with a scan rate of 5 mV s^{-1}.

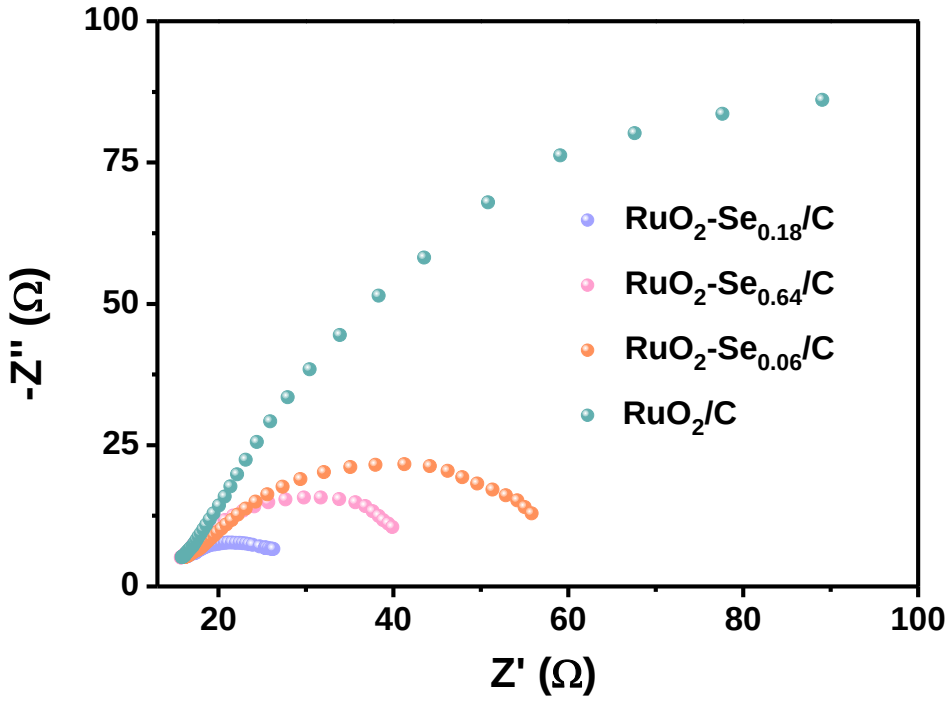

Figure S21. Electrochemical impedance spectroscopy (EIS) of RuO_2/C, RuO_2-$Se_{0.06}$/C, RuO_2-$Se_{0.18}$/C, RuO_2-$Se_{0.64}$/C.

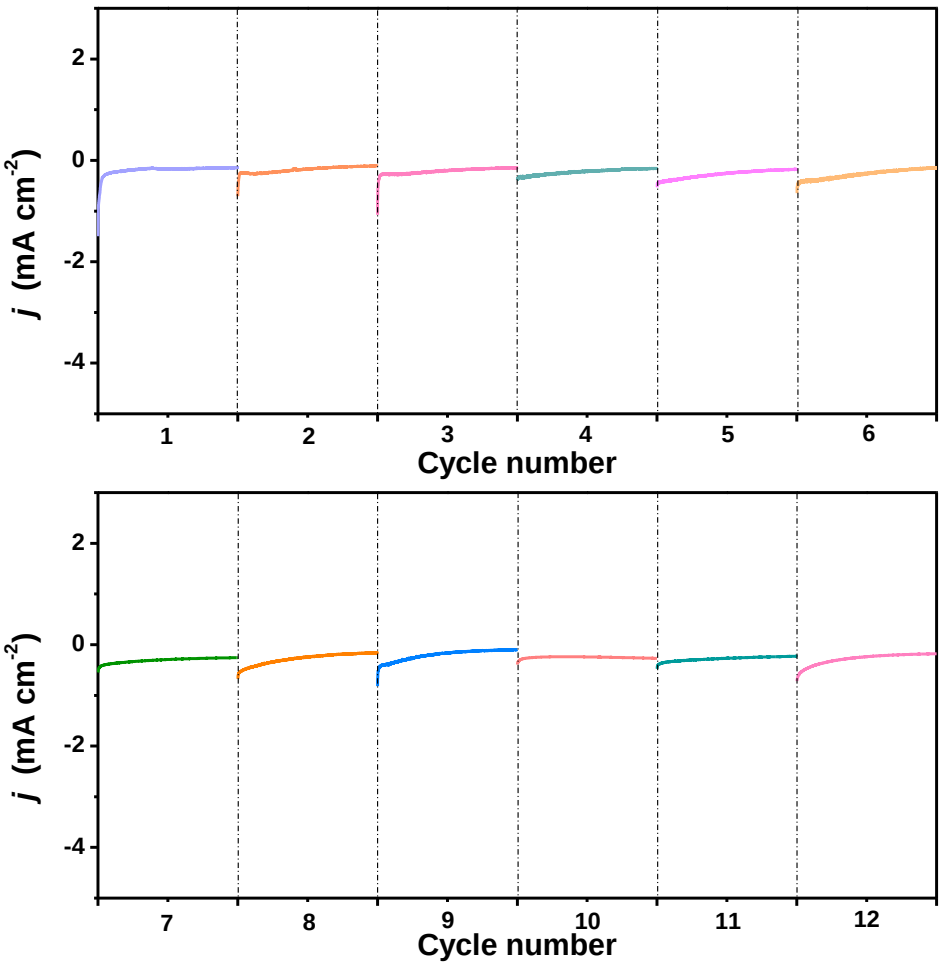

Figure S22. Time-dependent current density curves of RuO_2-$Se_{0.18}$/C with 1 h for each cycle in N_2-saturated 0.1 M Li_2SO_4.

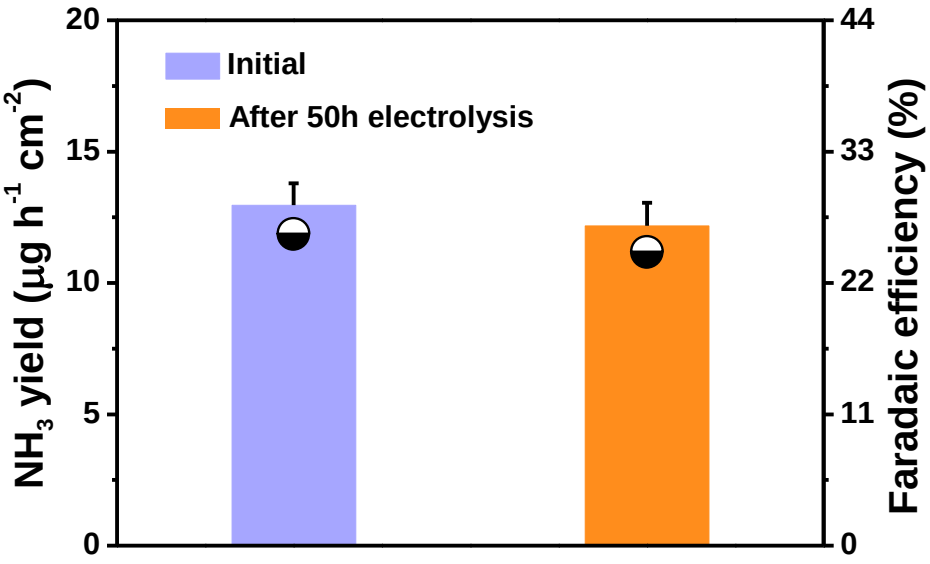

Figure S23. NH_3 yield and FE after charging at -0.1 V vs. RHE for 1h and 50 h.

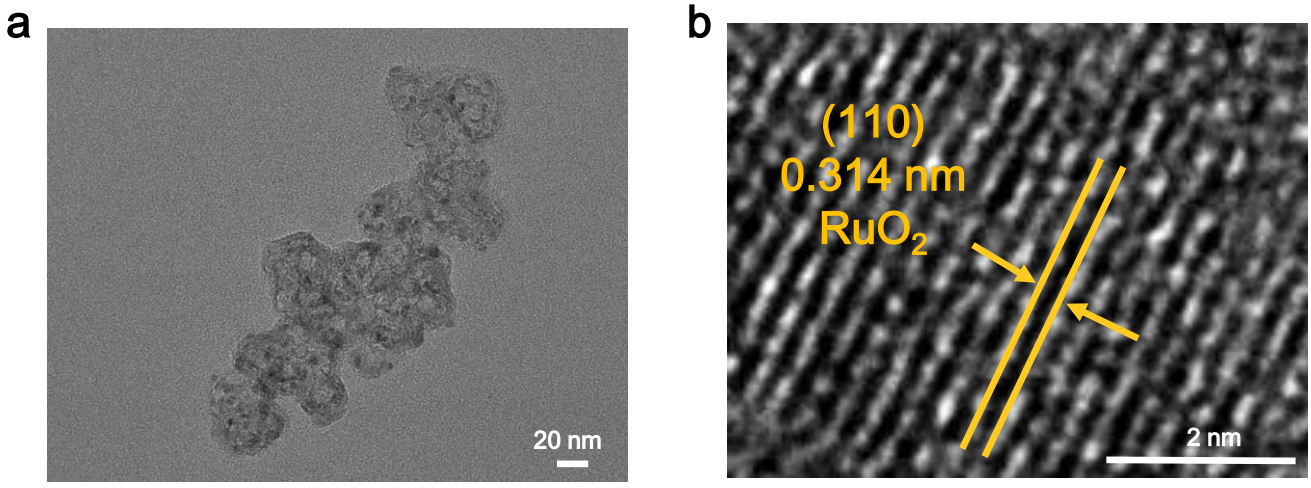

Figure S24. (a) The TEM image and (b) HRTEM image of RuO_2-$Se_{0.18}$/C catalyst after NRR.

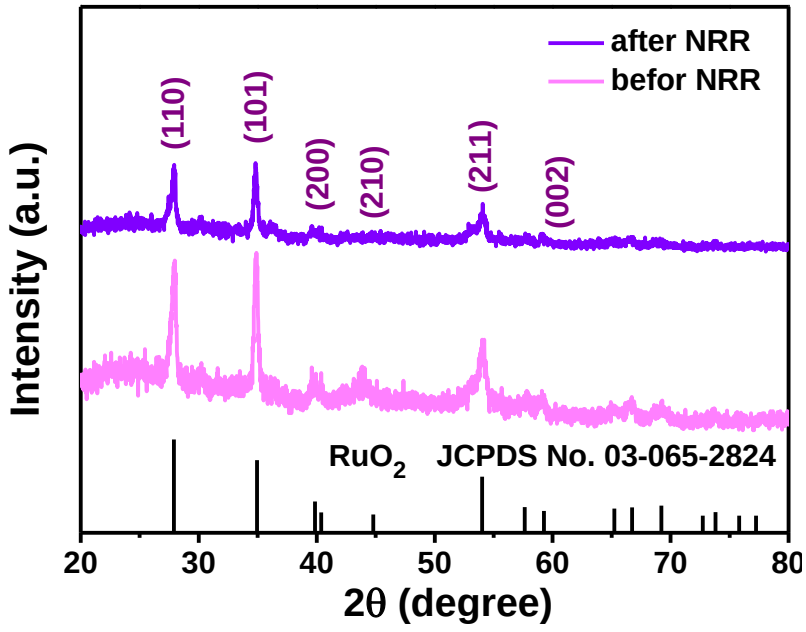

Figure S25. The XRD pattern of RuO_2-$Se_{0.18}$/C catalyst before and after NRR.

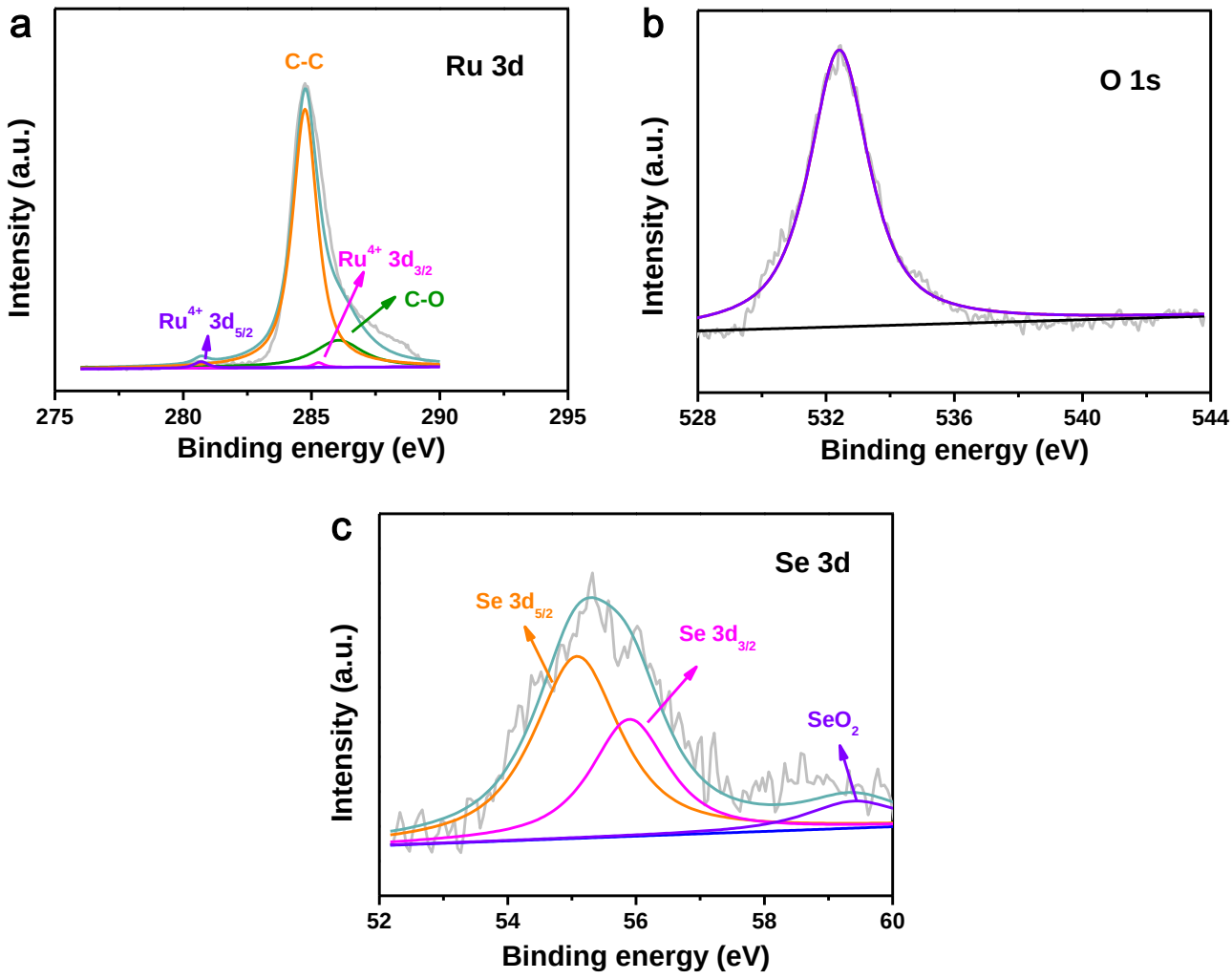

Figure S26. XPS spectra of (a) Ru 3d, (b) O 1s and (c) Se 3d signals in RuO_2-$Se_{0.18}$/C after time-dependent current density test.

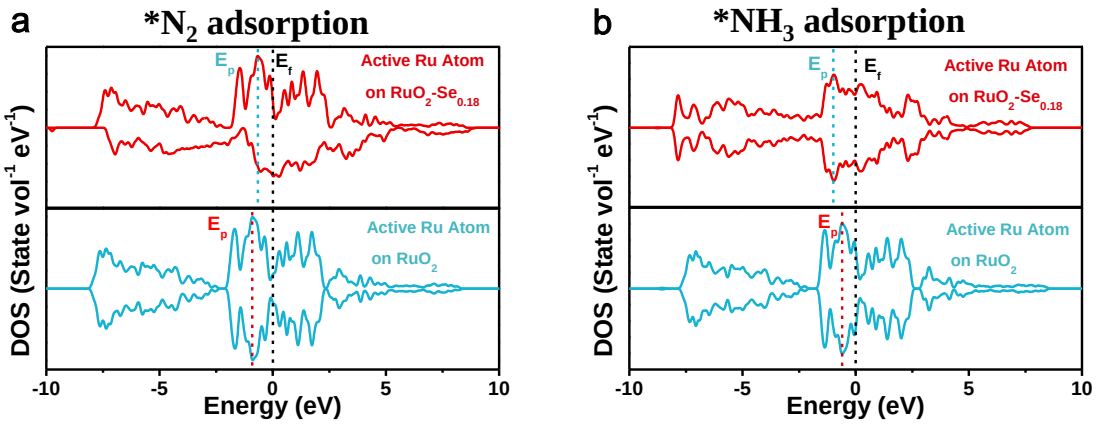

Figure S27. PDOS of active Ru atoms on RuO_2-$Se_{0.18}$ and RuO_2 upon (a) *N_2 adsorption and (b) *NH_3 adsorption.

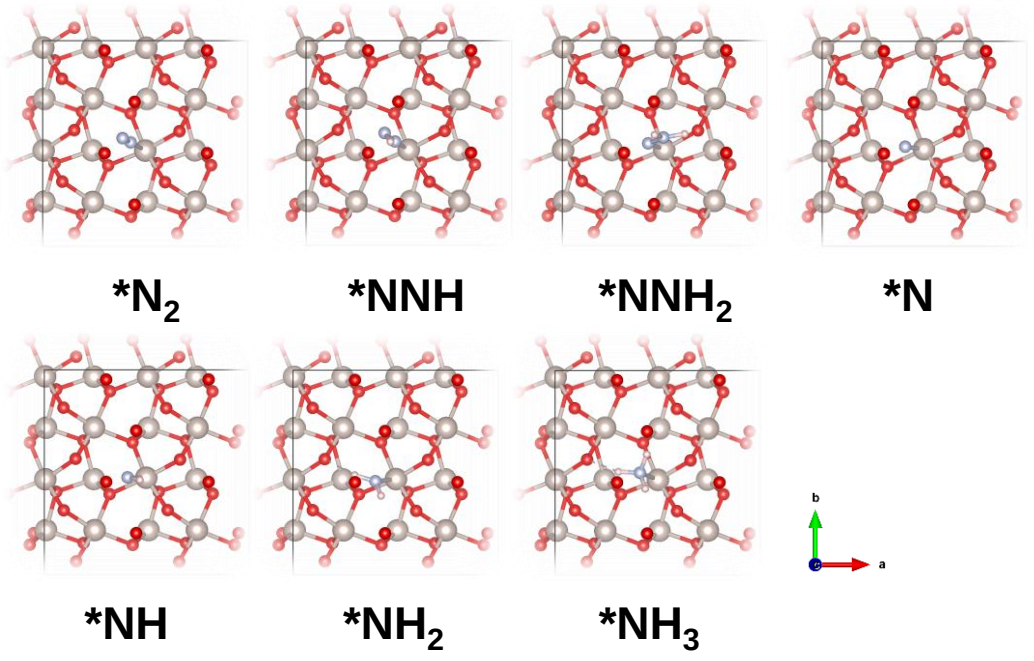

Figure S28. The reaction path carried out around the optimized geometry of the RuO_2 intermediate. Color code: pink, H; red, O; blue, N; gray, Ru.

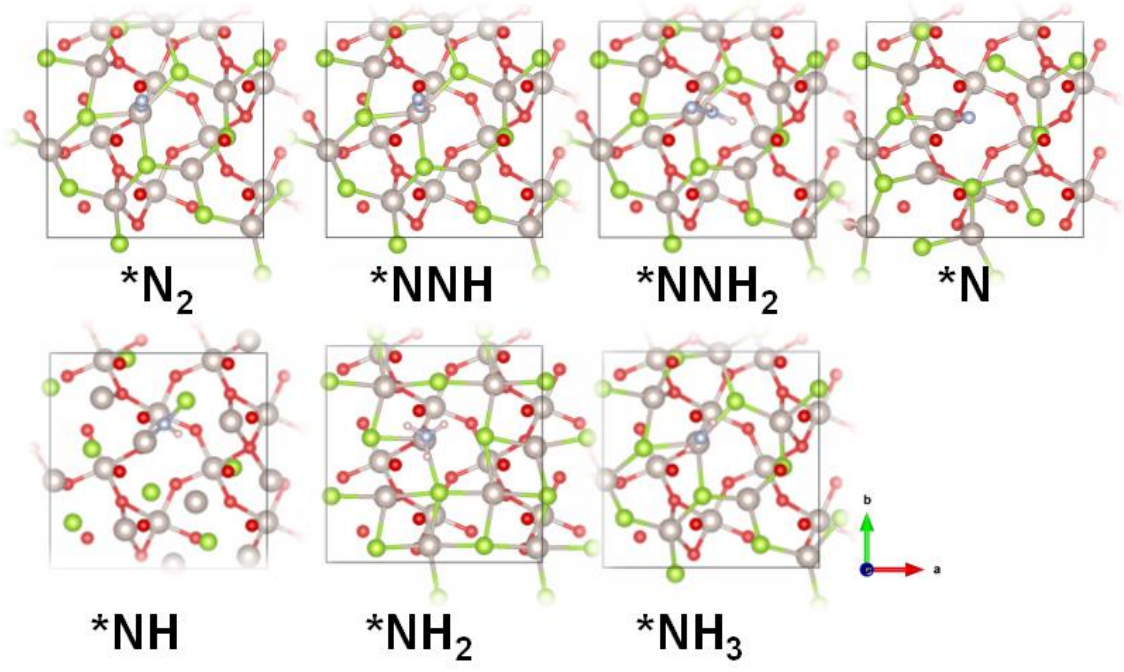

Figure S29. The reaction path carried out around the optimized geometry of the RuO_2-$Se_{0.18}$ intermediate. Color code: pink, H; red, O; blue, N; gray, Ru; green, Se.

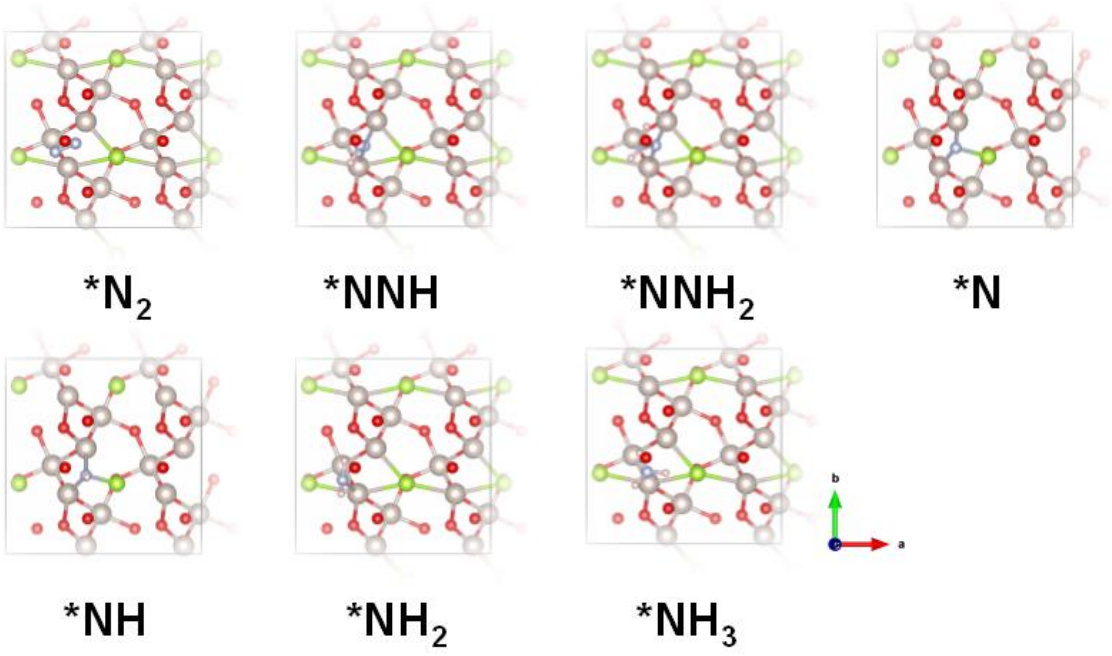

Figure S30. The reaction path carried out around the optimized geometry of the RuO_2-$Se_{0.06}$ intermediate. Color code: pink, H; red, O; blue, N; gray, Ru; green, Se.

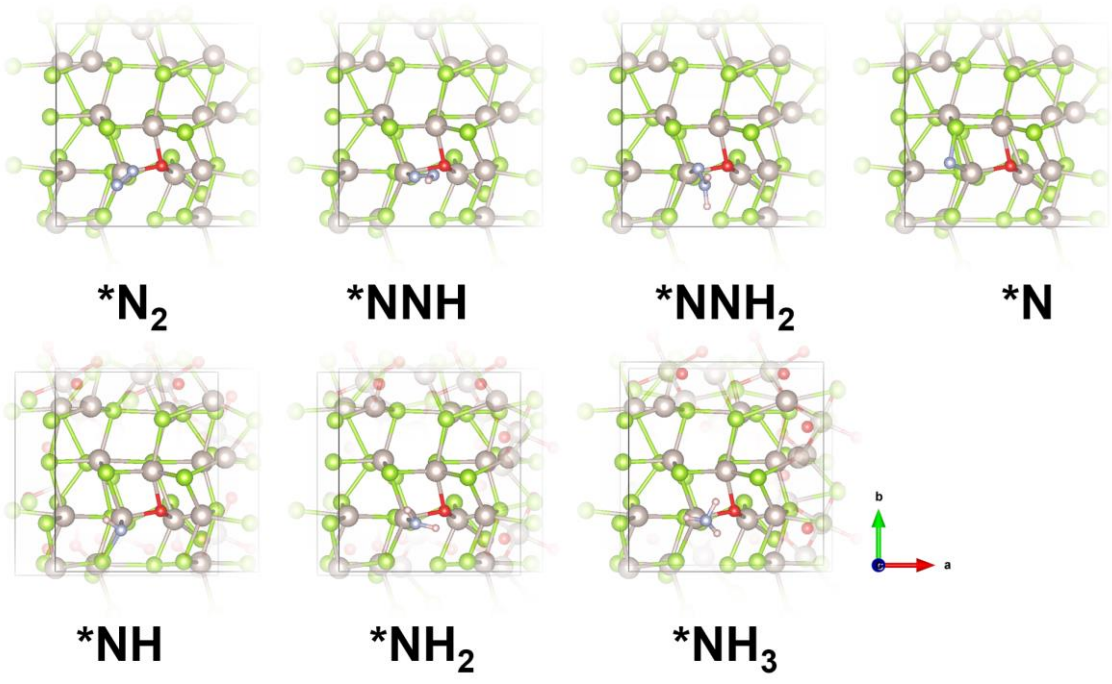

Figure S31. The reaction path carried out around the optimized geometry of the RuO_2-$Se_{0.64}$ intermediate. Color code: pink, H; red, O; blue, N; gray, Ru; green, Se.

Table S1. The comparable results of our work and other recently reported NRR catalysts at the following potentials.

Process	Catalyst	Conditions	Yield rate ($\mu g\ h^{-1}\ cm^{-2}$)	Faradaic efficiency (%)	Ref.
Electrocatalysis	RuO_2/C	0.1M Li_2SO_4 -0.1 V	1.6	10.45	This work
	RuO_2-$Se_{0.06}$/C	0.1M Li_2SO_4 -0.1 V	1.85	12.25	This work
	RuO_2-$Se_{0.18}$/C	0.1M Li_2SO_4 -0.1 V	12.97	26.01	This work
	RuO_2-$Se_{0.64}$/C	0.1M Li_2SO_4 -0.1 V	3.25	14.43	This work
	Ti_3C_2	0.1M KOH -0.1 V	0.5	21.3	[3]
	RO-Cu_3P/CFC	0.1M Na_2SO_4 -0.1 V	4.7	12.3	[4]
	FL-Sb	0.1M KOH -0.1 V	1.84	6.2	[5]
	MoS_2	0.1M KOH -0.1 V	8.35	16.1	[6]
	E_{ex}-COF/NC	0.1M KOH -0.1 V	7.1	34.9	[7]
	NV-W_2N_3	0.1M KOH -0.1 V	0.94	10.1	[8]
	Fe_{SA}-N-C	0.1M KOH -0.1 V	5.8	26.3	[9]
Haber-Bosch method	Fe/Ru-based catalysts	350~550 ℃, 200~300 atm	~20 % (N_2 conversion rate)	------	[10]
Biocatalysis	CdS:MoFe, N_2	------	321.3 $\mu g\ mg_{MoFe}^{-1}\ h^{-1}$	------	[11]

References

1. Zhang, L.; Ding, L.; Chen, G.; Yang, X.; Wang, H., *Angew. Chem. Int. Ed.* 2018, **58**, 2612-2642.
2. Zhu, X.; Wu, T.; Ji, L.; Li, C.; Wang, T.; Wen, S.; Gao, S.; Shi, X.; Luo, Y.; Peng, Q.; Sun, X., *J. Mater. Chem. A* 2019, **7**, 16117.
3. Xia, J.; Yang, S. Z.; Wang, B.; Wu, P.; Popovs, I.; Li, H.; Irle, S.; Dai, S.; Zhu, H., *Nano Energy* 2020, **72**, 104681.
4. Jin, M.; Zhang, X.; Han, M.; Wang, H.; Wang, G.; Zhang, H., *J. Mater. Chem. A* 2020, **8**, 5936-5942.
5. Bat-Erdene, M.; Xu, G. R.; Batmunkh, M.; Bati, A. S. R.; White, J. J.; Nine, M. J.; Losic, D.; Chen, Y.; Wang, Y.; Ma, T. Y.; Shapter, J. G., *J. Mater. Chem. A* 2020, **8**, 4735-4739.
6. Liu, Y.; Han, M.; Xiong, Q.; Zhang, S.; Zhao, C.; Gong, W.; Wang, G.; Zhang, H.; Zhao, H., *Adv. Energy Mater.* 2019, **9**, 1803935.
7. Liu, S.; Wang, M.; Qian, T.; Ji, H.; Liu, J.; Yan, C., *Nat. Commun.* 2019, **10**, 3898.
8. Jin, H.; Li, L.; Liu, X.; Tang, C.; Xu, W.; Chen, S.; Song, L.; Zheng, Y.; Qiao, S., *Adv. Mater.* 2019, **31**, 1902709.
9. Wang, M.; Liu, S.; Qian, T.; Liu, J.; Zhou, J.; Ji, H.; Xiong, J.; Zhong, J.; Yan, C., *Nat. Commun.* 2019, **10**, 341.
10. Van der Ham, C. J. M.; Koper, M. T. M.; Hetterscheid, D. G. H., *Chem. Soc. Rev.* 2014, **43**, 5183-5191.
11. Brown, K.; Harris, D.; Wilker, M.; Rasmussen, A.; Khadka, N.; Hamby, H.; Keable, S.; Dukovic, G.; Peters, J.; Seefeldt, L.; King, P., *Science* 2016, **352**, 448-450.